ChemPubSoc Europe

DOI: 10.1002/ejic.201800972

EurJIC European Journal of Inorganic Chemistry

Full Paper

POMs as Hydrogen Uptake Materials

CLUSTER ISSUE

Polyoxopalladates as Prototype Molecular Hydrogen Uptake Systems and Novel In situ Hydrogen Detectors on the Nanoscale

Carolin Schmitz-Antoniak,*[a] Natalya V. Izarova,[a] Nataliya Svechkina,[a] Alevtina Smekhova,[a] Maria Stuckart,[a] Detlef Schmitz,[b] and Paul Kögerler[c,d]

Abstract: Dodecapalladium(II) oxide-based molecular nanocubes encapsulating Fe^{3+} ($3d^5$) or Co^{2+} ($3d^7$) ions display facile hydrogen uptake with concurrent pronounced magnetization changes that suggests use as molecular hydrogen detection materials. Electronic and magnetic properties were investigated element-specifically by X-ray absorption spectroscopy and its associated magnetic circular and linear dichroisms. Hydrogenation reduces the Fe^{3+} ($3d^5$) ions to a $3d^6$ state while the Co^{2+} $3d^7$ configuration remains largely unaffected. However, in both cases, drastic changes of the crystal field and the magnetic properties were observed and quantified. The spin magnetic moments in the as-prepared state were obtained to be similar to the ones expected for free ions and are reduced significantly by about 30–40 % for both Fe and Co central ions upon loading with hydrogen. In addition, re-oxidation and hydrogenation in a second cycle were monitored and the sensitivity to hydrogen and oxygen exposure as a function of the peripheral capping groups is discussed.

Introduction

As an archetypical hydrogen storage metal, palladium stores hydrogen under ambient conditions.[1,2] In metallic palladium, the formation of two different Pd hydrides are reported, i.e. α-PdH_x and β-PdH_x, depending on the hydrogen content *x*. The hydrogen occupies interstitial sites of the face-centered cubic palladium[3] and although a hydrogen concentration of $x = 1$ seems to be possible in this structure, it has been found that the hydrogen loading saturates at about $x = 0.7$. At this concentration, the palladium lattice parameter is already increased from 0.389 nm by approximately 6 % and reaches values of about 0.402 nm.

For palladium nanoparticles, an even larger lattice constant of 0.404 nm has been reported[4] and discussed in terms of an enhanced hydrogenation of nanoparticles with respect to thin films or bulk material due to additional surface and subsurface adsorption sites.[5,6] Therefore, palladium at the nanoscale is a promising candidate for efficient hydrogen storage.

Polyoxopalladates form a new class of molecular palladium(II) oxide nanoscale materials with well-defined and tunable morphology that allows to tailor electronic and magnetic properties. The first example of this class, $[H_6Pd^{II}_{13}O_8(As^VO_4)_8]^{8-}$, was discovered in 2008[7] and is composed of a central palladium(II) ion surrounded by a distorted cubic shell of twelve palladium ions in square planar oxygen coordination environments and capped by eight arsenate heterogroups. A few years later, a novel family of polyoxopalladates was discovered with 3d and 4f transition metal ions in the center and various capping groups, e.g. phosphate[8] and phenylarsonate.[9,10] An overview of different structural types of polyoxopalladates and discussion about mutual influences between central ions and hosting shells can be found in the work of Yang and Kortz.[11] Here we investigated three different examples, two phosphate-capped and one phenylarsonate-capped: $[Co^{II}O_8Pd^{II}_{12}(P^VO_4)_8]^{14-}$ and $[Fe^{III}O_8Pd^{II}_{12}(P^VO_4)_8]^{13-}$ denoted as $CoPd_{12}P$ and $FePd_{12}P$, respectively, and $[Fe^{III}O_8Pd^{II}_{12}(PhAs^VO_3)_8]^{5-}$ denoted as $FePd_{12}PhAs$. Their molecular structures, as derived from their hydrated sodium salts, are sketched in Figure 1.

In this work, we explore the dodecapalladate nanocubes hosting 3d metal ions as hydrogen uptake materials whose H_2 charging is indicated by the magnetism of the central metal ions. [The palladium(II) oxophosphate/oxophenylarsonate shells themselves are diamagnetic.]

The influence of hydrogen loading on the magnetic properties has been studied by means of X-ray absorption spectroscopy. In particular, we investigated (i) the X-ray absorption

[a] *Peter-Grünberg-Institut (PGI-6), Forschungszentrum Jülich, 52425 Jülich, Germany*
E-mail: c.schmitz-antoniak@fz-juelich.de
http://www.csa-group.de
[b] *Helmholtz-Zentrum Berlin für Materialien und Energie, Albert-Einstein-Str. 15, 12489 Berlin, Germany*
[c] *Peter-Grünberg-Institut (PGI-6), Forschungszentrum Jülich, 52425 Jülich, Germany*
[d] *Institut für Anorganische Chemie, RWTH Aachen University, Landoltweg 1, 52074 Aachen, Germany*

Supporting information and ORCID(s) from the author(s) for this article are available on the WWW under https://doi.org/10.1002/ejic.201800972.

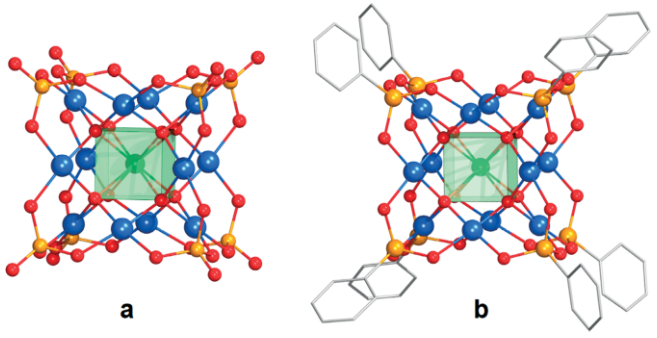

Figure 1. Molecular structure of the investigated polyoxopalladates: (a) Ball-and-stick representation of $MPd_{12}P$ (M = Co, Fe). The cubic environment of the central ion is emphasized by a green cube. Color legend: Pd blue, O red, P orange. (b) Ball-and-stick representation of $MPd_{12}PhAs$ (M = Fe). The cubic environment of the central ion is emphasized by a green cube. For the sake of clarity, phenyl groups are shown in a wire mode. Color legend: Pd blue, O red, As orange. H atoms are omitted for clarity.

near-edge structure (XANES) to monitor changes in the electronic structure, (ii) X-ray magnetic circular dichroism (XMCD) for the determination of effective spin and orbital magnetic moments, and (iii) X-ray magnetic linear dichroism (XMLD) for a refined analysis of crystal field splittings of the Fe and Co centers and their magnetic characteristics. These methods gave us the possibility to study electronic and magnetic properties element-specifically. In the main paper, we focus on the central 3d metal ions while further investigations on palladium, oxygen and capping group elements can be found in the Supporting Information. In addition, oxidation and reduction in a second cycle as well as the influence of capping groups, i.e. the phosphate or phenylarsonate groups, on the reactivity were monitored by XANES.

Results

Hydrogen was incorporated by a soft hydrogen plasma which is more efficient than H_2 gas. In this connection, soft means a low pressure plasma – frequently called cold plasma – with a low degree of ionization. It has been shown[12] that this treatment allows to reduce γ-Fe_2O_3 to Fe_3O_4 within 20–30 min which proves the low reactivity of this plasma. To ensure that no elements were removed by the plasma treatment, the XANES at the phosphorus L_1 absorption edge was measured in addition (see Supporting Information, Figure S1 and Table S1).

The fact that hydrogen modifies the physical properties of the palladates is immediately evident from color changes: Figure 2 shows photographs of the sodium salts of $CoPd_{12}P$ and $FePd_{12}P$ on highly oriented pyrolytic graphite (HOPG).

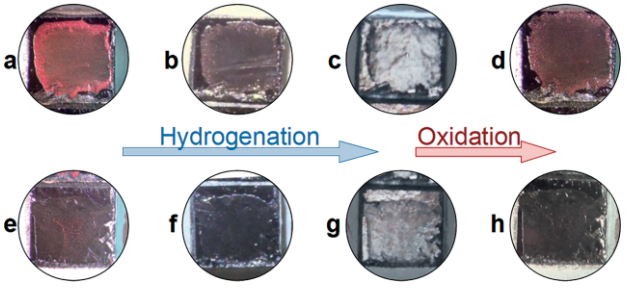

Figure 2. Color changes of Co/$FePd_{12}P$ due to hydrogen/oxygen treatment: Photographs of $CoPd_{12}P$ on HOPG substrate (upper row) and $FePd_{12}P$ on HOPG substrate (lower row) in the as-prepared state (a, e), after incomplete hydrogen loading (b, f), after full hydrogen loading (c, g), after subsequent exposure to air (d, h).

In the as-prepared state (a), $CoPd_{12}P$ had a red color. Upon loading with hydrogen, the color changed over brownish gray (b) to shiny gray (c). Particularly, the visual impression was very similar to the one of the clean HOPG substrate, thus, the hydro-

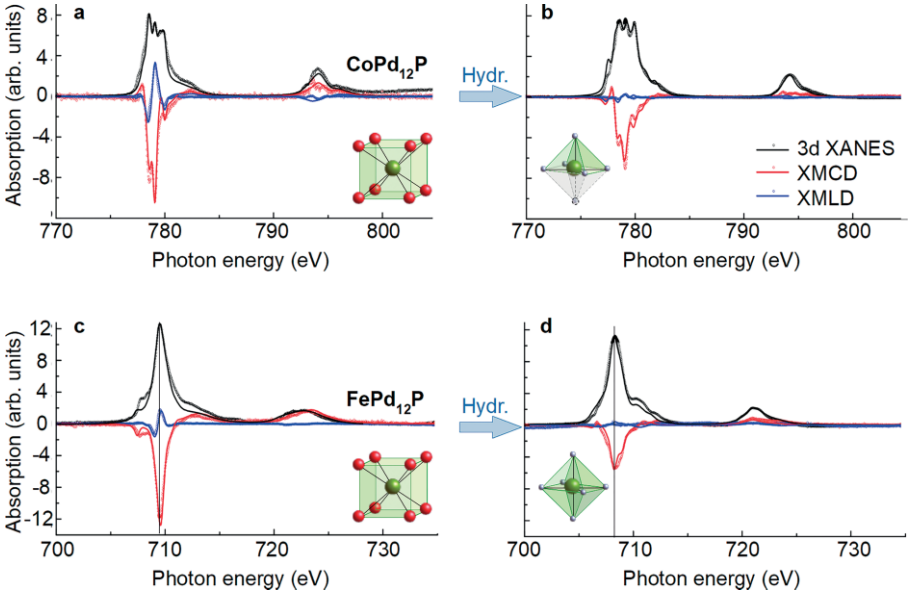

Figure 3. Calculated and experimental 3d XANES, XMCD, and XMLD for $CoPd_{12}P$ (top panels) and $FePd_{12}P$ (bottom panels) in the as-prepared state (a, c) and after hydrogenation (b, d). Open symbols refer to experimental data, solid lines refer to simulations for Co $3d^7$ and Fe $3d^5$/Fe $3d^6$, respectively. The insets sketch the local environment of the central 3d ion according to the crystal field.

genated samples were difficult to see. After exposure to air, the color changed again to reddish (d).

The distinct colors of the samples in the as-prepared and re-oxidized states indicate that these states were not equivalent. Thus, a second step of hydrogenation was performed to check the reproducibility. Again, the color changed to shiny gray for the hydrogen loaded state. For the brownish as-prepared $FePd_{12}P$ (e), the change of color was not so obvious, but still clearly visible. Particularly, the metallic appearance was also obtained for $FePd_{12}P$ after complete hydrogenation (g).

By analyses of the XANES, XMCD, and XMLD spectra, changes in the electronic structure and magnetic properties due to hydrogenation were investigated and quantified. The experimental spectra are shown in Figure 3 for $CoPd_{12}P$ (top panels) and $FePd_{12}P$ (bottom panels) before (a, c) and after (b, d) hydrogenation. To quantify the splittings of the energy levels caused by the crystal fields of the environment around the 3d metal ions, simulations were fitted to the experimental data by using the CTM4XAS program package.[13]

The major contribution to the crystal fields, in which the central 3d transition metal ions are placed, is caused by type, distance and coordination symmetry of nearest-neighbor atoms or ions. An indirect influence of the outer shell atoms in the palladate clusters is already included assuming that the values of the crystal fields in the simulations are effective values. For a better comparison with simulated spectra, the experimental XANES spectra were adjusted for electron transitions into higher unoccupied states or the continuum by subtraction of a two step-like function. The resulting signals correspond to electron transitions to the 3d states only and are denoted 3d XANES. The best fits are presented in Figure 3 as solid lines while the open symbols refer to experimental data taken at a temperature of 4.3 K in a magnetic field of 6 T. The crystal field splitting energies 10Dq and the nephelauxetic parameters β that had to be modified are presented in Table 1 and will be discussed in this work. All fitting parameters and line broadenings are summarized in the Supporting Information (Table S2).

Table 1. Properties of $CoPd_{12}P$ and $FePd_{12}P$ before and after different hydrogenation and oxidation steps, i.e. visual impression, central ions, crystal field splittings 10Dq, and the nephelauxetic parameters β for the central ions as determined from fitting simulated spectra to experimental XANES, XMCD, and XMLD. Full sets of parameters can be found in the Supporting Information (Table S2).

Sample	Visual impression	Central ion	10Dq [eV]	β
$CoPd_{12}P$	red	Co $3d^7$	−0.62 ± 0.05	0.9
$CoPd_{12}P$-H	metallic gray	Co $3d^7$	+0.80 ± 0.05[a]	0.7
$CoPd_{12}P$-H/O	reddish	Co $3d^7$	+1.1 ± 0.20	0.9
$CoPd_{12}P$-H/O/H	metallic gray	Co $3d^7$	+0.8 ± 0.10	0.7
$FePd_{12}P$	brown	Fe $3d^5$	−1.10 ± 0.05[b]	0.5
$FePd_{12}P$-H	metallic gray	Fe $3d^6$	+0.80 ± 0.05[a]	0.7
$FePd_{12}P$-H/O	brown	Fe $3d^5$	+1.5 ± 0.20	0.8
$FePd_{12}P$-H/O/H	metallic gray	Fe $3d^6$	+0.8 ± 0.10	0.7

[a] A distortion of up to Ds = −0.08 eV does not change the simulated spectra significantly. [b] An additional distortion of Dt = −0.06 eV was added.

In the case of $CoPd_{12}P$, only subtle changes in the fine structure of the XANES are visible after hydrogenation, in particular when comparing the intensities of the three main peaks at the Co L_3 absorption edge around 780 eV. The energy position and fine structures are typical for Co^{2+} ($3d^7$) ions. After hydrogenation, the intensity of the X-ray absorption is slightly reduced corresponding to an increased number of electrons in the final 3d states.

The reduction of the XMCD signal, which is proportional to the expectation value of the atomic magnetic moments along the direction of the magnetic field, is more significant and indicates smaller magnetic moments after hydrogenation than in the as-prepared state. However, in both cases the XMCD is sizeable corresponding to a high-spin state, that is supported by the large branching ratio of the 3d XANES, i.e. the ratio of the integrated absorption intensity at the L_3 edge to the total intensity, $A(L_3)/A(L_3 + L_2)$. Low-spin states exhibit smaller branching ratios on average.[14] Since the XMLD is proportional to the expectation value of the squared magnetic moments, its amplitude is significantly reduced as well after hydrogenation.

The Fe $L_{3,2}$ absorption edges of $FePd_{12}P$ are clearly shifted towards lower energies after hydrogenation indicating a change of the 3d electron configuration from $3d^5$ (Fe^{3+}) in the as-prepared state to $3d^6$. The magnetic moments are reduced as well as can be seen from the amplitudes of the magnetic dichroisms.

Calculated values of the effective spin and orbital magnetic moments obtained from a sum-rules[15–17] based analysis are summarized in Table 2 and discussed in more detail below.

Table 2. Magnetic properties of $CoPd_{12}P$ and $FePd_{12}P$ before and after hydrogenation, i.e. effective spin and orbital magnetic moments, total magnetic moment and relative change of the total magnetic moment upon hydrogenation as determined from XMCD of the central 3d ions at 4.3 K in a magnetic field of 6 T (about 90 % of magnetic saturation).

Sample	m_S^{eff}	m_L	m_{tot}	Δm_{tot}
	[μ_B/3d-atom]	[μ_B/3d-atom]	[μ_B/3d-atom]	
$CoPd_{12}P$	2.80 ± 0.56	0.53 ± 0.05	3.33 ± 0.61	
$CoPd_{12}P$-H	1.76 ± 0.35	0.53 ± 0.05	2.29 ± 0.40	−31 %
$FePd_{12}P$	4.09 ± 0.81	0.02 ± 0.01	4.11 ± 0.82	
$FePd_{12}P$-H	2.37 ± 0.47	0.20 ± 0.02	2.57 ± 0.49	−37 %

After hydrogenation, the samples were re-oxidized and a second hydrogenation treatment was performed. The corresponding 3d XANES after each preparation step are shown in Figure 4 for both samples together with the corresponding simulations. It can clearly be seen by the peak positions, that Co remains with its $3d^7$ electron configuration, while the central Fe ions change from $3d^5$ in the as-prepared and re-oxidized state to $3d^6$ after the first and second hydrogenation. The related energy positions are summarized in the Supporting Information (Table S3). Having a closer look to the spectral shape in the as-prepared and re-oxidized state, small differences can be seen for both Co and Fe states. They can be assigned to a change in the crystal field related to the surrounding oxygen ions.

To study a possible influence of the capping groups on the reduction and oxidation behavior of the polyoxopalladates, the XANES of $FePd_{12}P$ is compared to the XANES of $FePd_{12}PhAs$ in Figure 5 for the as-prepared state (upper panel), after hydrogenation (center) and after partial re-oxidation (lower panel). The samples have been only partially re-oxidized by exposure to O_2 gas to see the differences in the re-oxidation sensitivity more clearly.

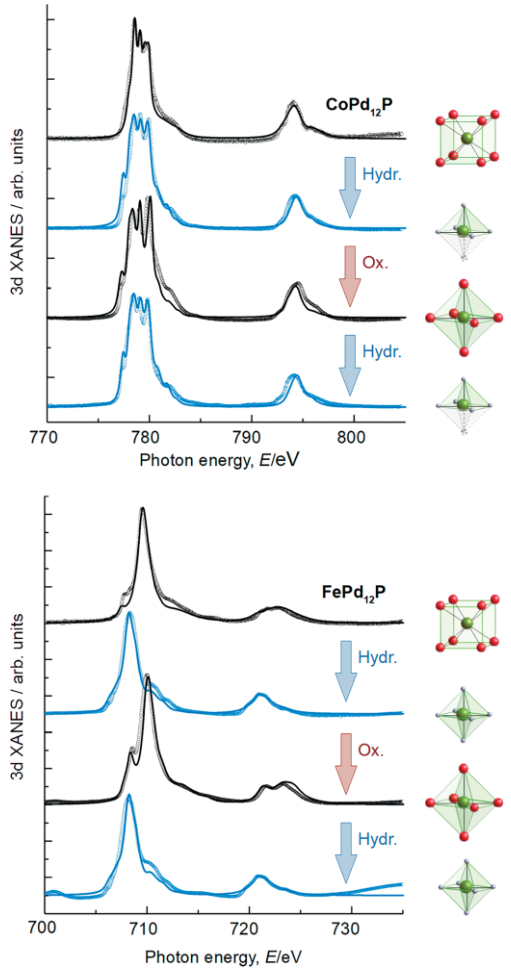

Figure 4. 3d XANES of $CoPd_{12}P$ (upper panel) and $FePd_{12}P$ (lower panel) after different hydrogenation/oxidation steps, i.e. in the as-prepared state, after hydrogenation, after subsequent re-oxidation, and subsequent second hydrogenation (from top to bottom). Open symbols refer to experimental data, solid lines refer to simulations. On the right, the local environments according to the crystal fields are depicted.

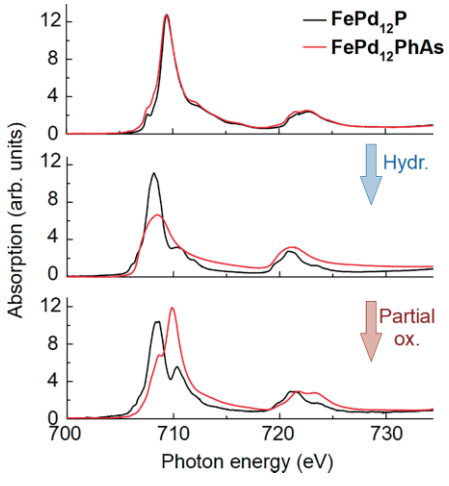

Figure 5. Comparison of experimental XANES of $FePd_{12}P$ (black line) and $FePd_{12}PhAs$ (red line) after different hydrogenation/oxidation steps, i.e. for the as-prepared state (upper panel), after hydrogenation (center) and after partial re-oxidation (lower panel).

While in the as-prepared state the spectral shapes of the XANES of $FePd_{12}P$ and $FePd_{12}PhAs$ are very similar, there are considerable differences after hydrogenation. The XANES of $FePd_{12}PhAs$ exhibits no fine structures and the branching ratio is close to the value of metallic Fe. However, the maxima of both XANES of $FePd_{12}P$ and $FePd_{12}PhAs$ are shifted to lower energies corresponding to a $3d^6$ configuration. After exposure to 4 hPa (4 mbar) of O_2 gas for 30 min, the samples are partially re-oxidized. For the $FePd_{12}P$ sample, the majority of Fe has still $3d^6$ configuration as can be seen from the energy position of the main peak. For the $FePd_{12}PhAs$ sample, the main peak is already shifted to higher energies typical for Fe $3d^5$. Only a more pronounced shoulder at lower energies indicates a small fraction of remaining Fe $3d^6$.

Discussion

In the following, the changes in the crystal field parameters and the electronic structure (particularly the nephelauxetic effect) due to hydrogenation and oxidation are discussed in more detail before turning to the discussion of the magnetic properties of the central 3d metal ions and the influence of capping groups on the sensitivity to hydrogen and oxygen.

Crystal Field Splitting Energies and 3d Occupation

In the as-prepared states, the splittings 10Dq are negative for both Co and Fe central ions, i.e. 10Dq = (–0.62 ± 0.05) eV and 10Dq = (–1.1 ± 0.05) eV, respectively (Table 1). The sign corresponds to the crystal field created by the eight oxygen ions in the cubic coordination environment around the metal center as sketched in Figure 1. In this geometry, the two e orbitals are lower in energy than the three t_2 orbitals, since the latter have a larger contribution pointing to the negatively charged oxygen ions connected to a larger Coulomb repulsion of the d electrons.

However, since none of the orbital lobes point directly to the oxygen ions, the absolute value of 10Dq is rather small stabilizing the high-spin configuration. For the case of Fe, a small primarily axial distortion had to be included by the crystal field parameter Dt = –0.06 eV, in particular to be able to simulate the XMLD. This is in agreement to the finding that there exists a zero-field splitting in electron paramagnetic resonance as reported earlier.[9] Introducing an even smaller additional distortion in the (*x*,*y*) plane could further improve the fitting, but was discarded here to keep the number of fitting parameters reliable. Since the crystal field splitting does not only depend on the symmetry and distance of the surrounding oxygen ions, but also on the charge of the central ion, the absolute value of the splitting is larger for the case of Fe^{3+} than for Co^{2+}.

After hydrogenation, the effective charge of the central ion is very similar for Fe and Co resulting in the same crystal field splitting. The positive sign of 10Dq indicates an octahedral crystal field, which means that after hydrogenation the three t_2 orbitals are lower in energy than the two e orbitals. A possible configuration in agreement to the obtained crystal fields, is the coordination of the central ion by six hydrogen atoms in octa-

hedral coordination environment. For Fe^{2+} hydrides, this configuration is typical while Co in a hydrogen environment more likely possesses a square-pyramidal coordination state with the formal oxidation state +1.[19,20] A square-pyramidal symmetry yields a further splitting of the threefold degenerate t_2 states into one single and one twofold degenerate state and a splitting of the twofold degenerated e states. This additional splitting has a considerable influence particularly on the XMLD. In fact, a splitting of up to Ds = –0.08 eV to model a square-pyramidal symmetry still leads to a reasonable agreement between simulation and experiment. The geometries are sketched as insets in Figure 3 d and b, respectively.

After re-oxidation the crystal field splitting is about 10Dq = (+1.5 ± 0.2) eV for the case of Fe $3d^5$ and (+1.1 ± 0.2) eV for Co $3d^7$ as determined from simulations of the XANES. The positive sign shows that the crystal field of the as-prepared state caused by the unusual eightfold coordination of the central ion, cannot be recovered. This is in agreement with the color change [Figure 1 (a) compared to (d)] and explains the differences in the spectral shape and slightly different energy positions of the main peaks in the XANES of the palladates in the as-prepared state and after re-oxidation of the hydrogenated state that can be seen in Figure 4.

In general, the good agreement between simulations and experimental data for the palladate samples shows that the simple description of a single ion placed in a crystal field sufficiently explains the spectral features obtained in X-ray absorption.

The stability of Co $3d^7$ is also in agreement with the absence of detectable electroactivity in voltammetry in similar polyoxopalladates[8] and heteropolytungstates[21] hosting $3d^7$ Co^{II} ions as well.

However, hydrogen is known to hybridize with the 3d electrons of transition metals leading to a band-like electronic structure and modified density of states. Indeed, the intensity of the Co $3d^7$ 3d XANES spectrum decreases after hydrogenation which indicates a larger number of 3d electrons (smaller number of unoccupied final 3d states). This decrease is about 5 %. For the case of Fe, the decrease is even larger (17 %) and is connected to a change of electron configuration from nominal $3d^5$ to $3d^6$.

If we use the 3d XANES intensity of Co $3d^7$ in the as-prepared $CoPd_{12}P$ as reference value corresponding to a number of unoccupied d states of $n_h^d = 3$, we find for Fe ions in the as-prepared $FePd_{12}P$ sample a number of unoccupied 3d states of about $n_h^d \approx 4.7$ (Supporting Information, Table S4), which is already slightly reduced with respect to the nominal value of 5.0. This may indicate a covalent contribution to the basically ionic bond.

Nephelauxetic Effect

The nephelauxetic effect denotes the spatial expansion of orbitals of a metal ion in a complex. This expansion reduces the Coulomb repulsion between electrons in the orbitals which is reflected by a reduction of the (normalized) Slater Condon parameters F_2 and F_4 (or Racah parameter $B = F_2 - 5F_4$) compared to its free ion value. For the d orbitals of the Co^{2+} ions in $CoPd_{12}P$, the reduction factor is $\beta = 0.9$, i.e. the Slater Condon parameters are reduced to 90 % of the value for the free ion. (Compared to the Hartree Fock value, they are reduced to 72 %, because the value of the free ion is reduced to 80 % with respect to the Hartree Fock value.)

For the Fe^{3+} ions in $FePd_{12}P$, the reduction factor is $\beta = 0.5$ (i.e. 40 % of the Hartree Fock value). The smaller value of β for Fe^{3+} compared to Co^{2+} is in agreement to the well-known nephelauxetic series for metal ions and may contain a further reduction caused by the covalent contribution to the bonding, which was concluded from the slightly reduced number of unoccupied 3d states.

After hydrogenation, the best fit to the absorption spectra of Co^{2+} ions was obtained for $\beta = 0.7$ in the simulations. The significant reduction with respect to the as-prepared state is connected to a further delocalization of the d electrons. This can be interpreted as a larger covalent contribution to the bond between the d metal and its surrounding ligands. For central Fe ions, β increases from 0.5 to 0.7 after hydrogenation. This increase is mainly caused by the change of the valence state from Fe^{3+} to Fe^{2+}. A delocalization of electrons and a more band-like electronic structure after hydrogenation is also supported by the color change of the material: In the as-prepared state, the red color of the $CoPd_{12}P$ is connected to the absorption of green light exciting electrons from the ground state into energetically well-defined excited states. In the case of Fe^{III} in oxidic ligand environments, intense ligand-to-metal charge transfer cause a more brownish color.

After hydrogenation, the occurrence of a band like structure with more delocalized electrons ("electron cloud") can also explain the change in the visual appearance towards metallic shiny gray (Figure 2c) that is related to the reflection of electromagnetic waves up to the frequency of the plasma frequency of delocalized electrons (and transmission for higher frequencies).

A third indication for electron delocalization is given by the branching ratios of the 3d XANES spectra. For both samples, the branching ratio in the as-prepared state is larger (0.83 ± 0.02) compared to the hydrogenated state (0.81 ± 0.02) as summarized in Table S4. Note that the uncertainty is related to the absolute values. The relative uncertainty is much smaller, so that the branching ratios after hydrogenation are clearly reduced in agreement to electronic delocalization.

For Fe $3d^5$, the expected branching ratio is larger than for Co $3d^7$ as it was experimentally obtained for a series of different 3d metal oxides.[22] A reduction of the branching ratio for Fe $3d^5$ to the value of Co $3d^7$ as found here can be explained again by covalent mixing.[14]

In summary, the visual impression, the reduced 3d XANES intensity, the reduced nephelauxetic parameters supported by the reduced branching ratios point to a delocalization of 3d electrons after hydrogenation. All these parameters suggest also for Fe in as-prepared $FePd_{12}P$ a covalent contribution to the bond by charge transfer.

Magnetism of Central 3d Ions

From magnetic field and temperature dependent magnetometry data shown in the Supporting Information (Figure S2), it

can be concluded that the magnetic moments determined at a temperature of 4.3 K in a magnetic field of 6 T are already close to the saturation values, i.e. about 90 % of the saturation value assuming that the dependence can be described by a Brillouin function.

To quantify effective spin and orbital magnetic moments of Co and Fe in our samples from XMCD spectra, sum-rules[15–17] based analyses were performed. The values of the effective spin magnetic moments were corrected for systematic uncertainties by a factor of 1.1. Details of the data treatment, the calculation of magnetic moments and discussion of the correction factors according to Piamonteze et al.[18] can be found in the Supporting Information.

The calculated values are summarized in Table 2. For the case of Co $3d^7$ in the as-prepared state, the spin magnetic moment of (2.80 ± 0.56) μ_B is in agreement to the saturation value expected for the free ion (3 μ_B), while the orbital magnetic moment is partially quenched in the cubic crystal field, but still sizeable [(0.53 ± 0.05) μ_B]. Hydrogenation leads to a significant decrease of the effective spin magnetic moment to (1.76 ± 0.35) μ_B. The orbital magnetic moment remains unchanged within experimental uncertainties. For the case of Fe $3d^5$ in the as prepared state, the spin magnetic moment of (4.09 ± 0.81) μ_B is also close to the saturation value expected for the free ion (5 μ_B). The same holds for the orbital magnetic moment that is close to zero as expected for the half-filled 3d shell of the high-spin $3d^5$ configuration. After hydrogenation, the resulting Fe $3d^6$ has a smaller spin magnetic moment than the corresponding free ion, i.e. (2.37 ± 0.47) μ_B compared to 4 μ_B. The orbital magnetic moment increased significantly to (0.20 ± 0.02) μ_B, which is still much smaller than the value for the free ion indicating again a partial quenching of the orbital moment.

For both Co and Fe central ions, the spin magnetic moments decrease significantly after hydrogenation by around 40 %. Since the spin magnetic moment is the dominating contribution to the technologically relevant total magnetic moment, the latter exhibits a distinct decrease as well, i.e. 30–40 %.

It is already known that hydrogen loading influences the magnetic moments of transition metal clusters[23–25] and thin films[26] due to an electron transfer from hydrogen to the 3d metal. As mentioned above, we found several indications for a charge transfer to the Co or Fe central ion in this work as well. For both Co $3d^7$ and Fe $3d^5$ any additional 3d electron has to have a minority spin reducing the net magnetic moment. This reduction is even larger than expected from simple electron counting which indicates that hydrogen leads to a more band like structure with a modified density of 3d states.

Thus, the significant reduction of the total magnetic moment after hydrogenation is related to the changes in the electronic structure and makes the central 3d metal ion a suitable monitor for the hydrogen loading.

Influence of Capping Groups

As previously suggested,[8] the bond lengths between the central 3d metal ion and the surrounding oxygen ions are influenced not only by the size of the central ion, but can be tuned by the prosthetic capping groups at the outside of the MPd_{12} cluster. As a rule of thumb one may note that shorter bonds of the capping groups cause a shrinking of the dodecapalladate nanocube hosting the central ion. For $FePd_{12}P$ the bond length between the Fe ion and the surrounding oxygen ions is 2.206(8) Å[8] and for $FePd_{12}PhAs$ it is 2.224(5) Å,[9] which is about 1 % larger.

From our results, this larger bond length is related to a more efficient reduction of the Fe $3d^5$ ion to $3d^6$. The shape and branching ratio of the XANES spectra clearly reminds of metallic Fe which may indicate the formation of metallic $FePd_{12}$ clusters.

By cyclic voltammetry, the reduction of Fe $3d^5$ central ions was already studied for polyoxopalladates in solution with different capping groups, in particular the phosphate[8] and phenylarsonate groups[9] used also in this work and selenite (SeO_3) groups.[9] The selenite capped system is denoted $FePd_{12}Se$ in this discussion. Interestingly, the voltage needed for the reduction of Fe $3d^5$ in $FePd_{12}PhAs$ and in $FePd_{12}P$ is roughly the same. However, significantly reduced bond lengths between the central ion and the oxygen ions occur in $FePd_{12}Se$ [2.149(16) Å]. The reduced bond length leads to a higher energy of the lowest unoccupied molecular orbital (LUMO) and thus, higher absolute values of the voltage needed for reduction had to be applied.[9] This finding qualitatively supports our result that the reduction is less efficient for the sample with shorter bonds of the central ion.

The same behavior was observed for the case of Co central ions. While in the as-prepared state, there are only small differences in the electronic and magnetic properties between $CoPd_{12}P$ and $CoPd_{12}PhAs$,[27] the hydrogenation is more efficient for the sample with PhAs capping groups as shown in the Supporting Information (Figure S6).

To see changes in the re-oxidation behavior more clearly, we present spectra after partial re-oxidation in Figure 5. It is obvious that also the re-oxidation is less efficient for $FePd_{12}P$ with the shorter bond lengths. This gives the opportunity to tailor the sensitivity of the central ion to hydrogen and oxygen, respectively, by choosing the right capping groups. For a higher sensitivity, capping groups with longer bonds shall be considered that allows also for longer bond length in the center of the dodecapalladate nanocube.

Conclusions

Although polyoxopalladates of the type $[MO_8Pd^{II}_{12}(RXO_m)_8]^{n-}$ hosting single 3d metals ions in their centers do not recover their initial state after a full hydrogenation-oxidation cycle, they can be considered as new hydrogen uptake and detection materials, whose charging state can be detected visibly and read out directly by its magnetization. Significant changes of about –30 to –40 % of the total magnetic moments were found for both Fe and Co ions upon hydrogen loading and are easy to detect. The change of the magnetic properties is accompanied by modifications of the electronic structure, that are in detail (i) reduction of the central ion, (ii) hybridization of the d states of the central ion with hydrogen s states, and (iii) a resulting more band like electronic structure which strongly modifies also the

visual appearance. The sensitivity of the system to hydrogen (and oxygen) can be tailored by the capping groups. As a rule of thumb, higher sensitivity can be achieved by capping groups RXO_3 with longer X–O bond lengths. The irreversible modifications of the molecular and electronic structure and related properties due to hydrogenation can also be turned to advantage by using thin films of polyoxopalladates as witness samples e.g. in hydrogen plasma cleaning applications.

In addition, this system can be used as a reference system to study the response of well-defined Co^{2+}, Fe^{3+} states in experimental methods and – with PhAs capping groups – as precursors for metallic clusters.

Experimental Section

Sample Preparation

$CoPd_{12}P$, $FePd_{12}P$, $FePd_{12}PhAs$, and $CoPd_{12}PhAs$ samples have been prepared according to the reported procedures[8,9] and characterized by IR spectroscopy. For X-ray absorption spectroscopy (XAS) measurements, freshly cleaved pieces of highly oriented pyrolytic graphite (HOPG) were used as substrates. The powder samples were solved in water and drop-coated on HOPG substrates mounted on a sample plate. To evaporate the water, the solutions were dried on a hot plate for a few minutes at a temperature of about 50 °C. This temperature is sufficiently low to avoid any thermal decomposition of the clusters. To ensure that samples compared in this work have been equally treated and are measured under the same conditions, two samples were mounted on the same sample plate, i.e. $FePd_{12}P$ and $CoPd_{12}P$ to study the influence of hydrogenation and oxidation on the central ions of these samples and $FePd_{12}P$ and $FePd_{12}PhAs$ to study the influence of capping groups on the sensitivity to hydrogen and oxygen, respectively.

Supporting measurements of hydrogenated $CoPd_{12}PhAs$ were carried out with two additional reference samples mounted on the sample plate, i.e. $CoPd_{12}P$ and $FePd_{12}PhAs$, to ensure reproducibility of the plasma treatment.

X-ray Absorption Spectroscopy

X-ray absorption spectroscopy measurements were carried out in the high-field endstation at the beamline UE46-PGM1 of the HZB-BESSYII synchrotron radiation facility in photon energy ranges of 680 eV ≤ E ≤ 780 eV for Fe $L_{3,2}$ absorption edges and 760 eV ≤ E ≤ 840 eV for Co $L_{3,2}$ absorption edges. XMCD spectra were corrected for the degree of circular polarization of 90 %. The samples were cooled down to the lowest temperature of about 4.3–4.5 K and magnetic dichroisms were measured in magnetic fields up to 6 T. The absorption was detected in total electron yield (TEY) mode by measuring the sample drain current. X-ray magnetic circular dichroism (XMCD) was measured as the difference of the absorption intensity of left and right circularly polarized X-rays under normal incidence with the magnetic field applied parallel to the k vector of incoming X-rays, see Equation (1):

$$I_{XMCD} = I_R - I_L \quad (1)$$

For the magnetic linear dichroism (XMLD), spectra with two different orientations of the X-rays' electric field vector are needed, i.e. parallel and perpendicular to the direction of applied magnetic field, see Equation (2):

$$I_{XMLD} = I_\perp - I_\parallel \quad (2)$$

This was realized by rotating the magnetic field by 90° and using horizontally and vertically polarized X-rays. However, in this geometry, the TEY is suppressed by the Lorentz force. Thus, the sample had to be rotated by a few degrees (between 15° and 28°) so that the magnetic field is no longer applied in the sample plane. Since no natural dichroism is expected for randomly oriented palladates, this should not influence the results.

The X-ray absorption near-edge structure (XANES) was obtained by averaging spectra taken with left and right circularly polarized X-rays and $I_\parallel$, see Equation (3):

$$I_{XANES} = (I_L + I_R + I_\parallel)/3 \quad (3)$$

Special care was taken to correct the different background signal for the two measurement geometries. Details about the data treatment can be found in the Supporting Information.

Plasma Treatment

A soft hydrogen plasma treatment was performed in situ in the preparation chamber at the beamline with a portable plasma chamber attached. The samples were placed about 20 cm away from the main plasma zone. The inductively coupled plasma was stabilized and optimized using a suitable matchbox for radio frequencies so that no reflected power was detected. The plasma was operated at a power of 20 W for two hours at a pressure of 2.0–2.8 Pa (1 Pa = 10^{-2} mbar).

CTM4XAS Simulations

Simulations were carried out using the CTM4XAS program package. This semi-empirical program is based on a Hartree–Fock method corrected for correlation effects to solve the atomic Hamiltonian.[28] It includes the core and valence spin-orbit coupling, the core-valence two-electron integrals (multiplet effects) and the effects of strong correlations within the charge-transfer model. In the case of metal ions in oxygen coordination environment, this approach is known to give reliable results. More details about the program and some examples of applications can be found, for example, in the papers of Stavitski and de Groot[13] and de Groot et al.[29]

For all samples studied here, the Slater integrals had to be reduced to 90–50 % of the atomic values. The instrumental line broadening is 0.1 eV and the life-time broadening was set to values between 0.16 and 0.8 eV depending on the sample. A detailed list of all parameters for $FePd_{12}P$ and $CoPd_{12}P$ before and after different hydrogenation and oxidation steps can be found in the Supporting Information.

The simulated XANES was fitted to the experimental data by a scaling factor. Simulated XMCD and XMLD spectra were scaled by the same factor and an additional factor (m and m^2 for the case of XMCD and XMLD, respectively), to account for the magnetic non-saturation of the samples.

Acknowledgments

We thank the Helmholtz-Zentrum Berlin (HZB) for the allocation of synchrotron radiation beamtime and access to the laboratory for magnetic measurements of the CoreLab Quantum Materials. For kind support we thank the HZB staff, particularly E. Weschke, E. Schierle, and K. Siemensmeyer. F. M. Römer and S. Salamon (U. Duisburg-Essen) are gratefully acknowledged for

help in construction of the plasma chamber and pre-characterization of the plasma. This work was funded by the Helmholtz Association (Young Investigator's Group Borderline Magnetism under contract no. VH-NG-1031).

Keywords: X-ray absorption · Magnetic properties · Polyoxometalates · Hydrogen

[1] T. Graham, *Philos. Trans. R. Soc. London* **1866**, *156*, 399.
[2] J. R. Lacher, *Proc. R. Soc. London Ser. A* **1937**, *161*, 525.
[3] A. Maeland, T. B. Flanagan, *Platinum Met. Rev.* **1966**, *10*, 20.
[4] M. Khanuja, B. R. Mehta, P. Agar, P. K. Kulriya, D. K. Avasthi, *J. Appl. Phys.* **2009**, *106*, 093515.
[5] C. Sachs, A. Pundt, R. Kirchheim, M. Winter, M. T. Reetz, D. Fritsch, *Phys. Rev. B* **2001**, *64*, 075408.
[6] J. A. Eastman, L. J. Thompson, B. J. Kestel, *Phys. Rev. B* **1993**, *48*, 84.
[7] E. V. Chubarova, M. H. Dickman, B. Keita, L. Nadjo, F. Miserque, M. Mifsud, I. W. E. C. Arends, U. Kortz, *Angew. Chem. Int. Ed.* **2008**, *47*, 9542; *Angew. Chem.* **2008**, *120*, 9685.
[8] M. Barsukova-Stuckart, N. V. Izarova, R. Barrett, Z. Wang, J. van Tol, H. W. Kroto, N. S. Dalal, B. Keita, D. Heller, U. Kortz, *Chem. Eur. J.* **2012**, *18*, 6167.
[9] M. Barsukova-Stuckart, N. V. Izarova, R. Barrett, Z. Wang, J. van Tol, H. W. Kroto, N. S. Dalal, P. Jiménez-Lozano, J. J. Carbó, J. M. Poblet, M. S. von Gernler, T. Drewello, P. de Oliviera, B. Keita, U. Kortz, *Inorg. Chem.* **2012**, *51*, 13214.
[10] M. Barsukova, N. V. Izarova, R. Ngo Biboum, B. Keita, L. Nadjo, V. Ramachandran, N. S. Dalal, N. S. Antonova, J. J. Carbó, J. M. Poblet, U. Kortz, *Chem. Eur. J.* **2010**, *16*, 9076.
[11] P. Yang, U. Kortz, *Acc. Chem. Res.* **2018**, *51*, 1599.
[12] C. Schmitz-Antoniak, D. Schmitz, A. Warland, N. Svechkina, S. Salamon, C. Piamonteze, H. Wende, *Sci. Rep.* **2015**, *6*, 20897.
[13] E. Stavitski, F. M. F. de Groot, *Micron* **2010**, *41*, 687694.
[14] B. T. Thole, G. van der Laan, *Phys. Rev. B* **1988**, *38*, 3158.
[15] B. T. Thole, P. Carra, F. Sette, G. van der Laan, *Phys. Rev. Lett.* **1992**, *68*, 1943.
[16] P. Carra, B. T. Thole, M. Altarelli, X. Wang, *Phys. Rev. Lett.* **1993**, *70*, 694.
[17] C. T. Chen, Y. U. Idzerda, H.-J. Lin, N. V. Smith, G. Meigs, E. Chaban, G. H. Ho, E. Pellegrin, F. Sette, *Phys. Rev. Lett.* **1995**, *75*, 152.
[18] C. Piamonteze, P. Miedema, F. M. F. de Groot, *Phys. Rev. B* **2009**, *80*, 184410.
[19] R. Bau, M. H. Drabnis, *Inorg. Chim. Acta* **1997**, *259*, 27.
[20] R. B. King, *Coord. Chem. Rev.* **2000**, *200–202*, 813.
[21] M. Ammam, B. Keita, L. Nadjo, I.-M. Mbomekalle, J. Fransaer, *J. Electroanal. Chem.* **2010**, *645*, 65.
[22] T. G. Sparrow, B. G. Williams, C. N. R. Rao, J.-M. Thomas, *Chem. Phys. Lett.* **1984**, *108*, 547.
[23] C. Ashman, S. N. Khanna, M. R. Pederson, *Chem. Phys. Lett.* **2003**, *368*, 257.
[24] N. O. Jones, M. R. Beltran, S. N. Khanna, T. Baruah, M. R. Pederson, *Phys. Rev. B* **2004**, *70*, 165406.
[25] P. Bessarab, in *The Effect of Hydrogen on the Magnetic Properties of Supported Nano Scale Clusters*, Magister Scientiarum thesis, University of Iceland, Reykjavik, **2009**.
[26] G. J. Mankey, M. T. Kief, F. Huang, R. F. Willis, *J. Vac. Sci. Technol. A* **1993**, *11*, 2034.
[27] M. Stuckart, N. Izarova, J. van Leusen, A. Smekhova, C. Schmitz-Antoniak, H. Bamberger, J. van Slageren, B. Santiago-Schübel, P. Kögerler, *Chem. Eur. J.* **2018**, accepted.
[28] R. D. Cowan, in *The Theory of Atomic Structure and Spectra*, University of California Press: Berkeley, **1981**.
[29] F. M. F. de Groot, J. C. Fuggle, B. T. Thole, G. A. Sawatzky, *Phys. Rev. B* **1990**, *42*, 54595468.

Received: August 13, 2018